LANGMUIR

pubs.acs.org/Langmuir Article

Unraveling the Structural Evolution of Aluminum Polyoxocations in Solution

Qi Zhao, Minjuan Zhao, Xiuling Jiao, Yuguo Xia,* and Dairong Chen*

Cite This: *Langmuir* 2024, 40, 20284−20293 Read Online

ACCESS | Metrics & More | Article Recommendations | Supporting Information

ABSTRACT: The primary objective within the realm of aluminum solution chemistry is to elucidate the structural changes in aluminum polyoxocations under the influence of altered solution conditions. Notably, previous reports are primarily focused on specific types, such as aluminum monomers, species from the Keggin series, and the planar Flat-Al_{13}^{15+} (F-Al_{13}) cluster. As a result, there is a lack of comprehensive understanding of the remaining aluminum polyoxocations and their respective transformation pathways. In response to this lack, we adopt a combined experimental and theoretical approach to explore the spectral properties of aluminum polyoxocations. Specifically, we analyze infrared spectra, Raman spectra, and aluminum-27 nuclear magnetic resonance (^{27}Al NMR) spectra. Notably, the changes in the spectral features originate from varying solution basicity levels. Through our findings, we can categorize the Al−O clusters into three primary groups: $Al(H_2O)_6^{3+}$ (Al_1), ε-Keggin-$[AlO_4Al_{12}(OH)_{24}(H_2O)_{12}]^{7+}$ (ε-Al_{13}), and 6-coordinated aluminum species. Notably, the Raman spectra exhibit prominent peak shifts at 559 and 595 cm^{-1}, indicating the existence of $Al_3(1)$ intermediates during the transition from the Al monomer to the ε-Al_{13} cluster. Overall, this paper presents a comprehensive summary of the possible mechanisms that govern the formation of ε-Al_{13} from $Al_3(1)$, offering a clearer picture of the aluminum polyoxocation landscape and its dynamics under various solution conditions.

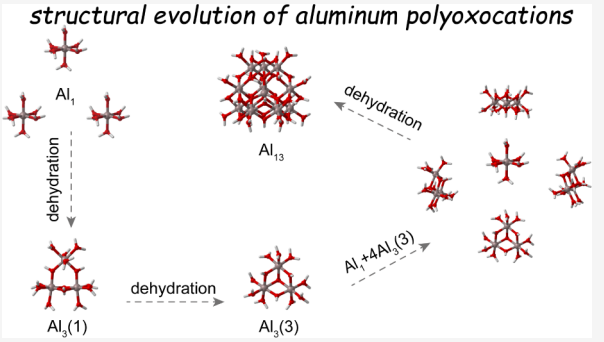

INTRODUCTION

The hydrolytic behavior of aluminum in aqueous solutions is of critical interest within the fields of geochemistry, environmental sciences, and materials chemistry.[1,2] The sol−gel technique is extensively utilized in the production of diverse aluminum-based products.[3] In this process, the product is significantly affected by the speciation and multiplicity of aluminum polyoxocations.[4] Since these species largely dictate the physicochemical characteristics of the resulting alumina sol and the subsequent aggregation framework of the alumina gel.[5] Furthermore, the nanoscale aluminum polyoxocations generated through hydrolysis can be used for flocculants, adsorptive materials, pillaring substances, and surface-active agents.[6] Hence, it is crucial to fully understand the fundamental characteristics and formation of different aluminum polyoxocations that occur during the hydrolysis and polymerization of aluminum salts. In particular, it is essential to advance the application and innovation within these pivotal chemical processes.

Nevertheless, the subnanometer dimensions of these multifarious aluminum polyoxocations render the precise discernment and assignment of emanating spectral features markedly challenging.[7] The structural diversity of aluminum polyoxocations makes it challenging to develop a robust theoretical framework that can effectively describe their formation and transformation processes.[8] The majority of aluminum polyoxocations is thermodynamically unstable, leading to dynamic behavior in solution, which makes it challenging to identify them experimentally.[9,10] Moreover, the intricate balance of thermodynamic equilibria among diverse aluminum polyoxocations significantly undermines the reliability of using additives to identify specific species.[11,12] Hence, achieving the in situ detection of these aluminum polyoxocations within aqueous solutions has emerged as a critical endeavor, one that is essential for demystifying their evolutionary pathways.

Currently, the predominant analytical techniques for probing aluminum polyoxocations in aqueous media include aluminum-27 nuclear magnetic resonance spectroscopy (^{27}Al NMR), the ferron colorimetric method, and electrospray ionization mass spectrometry (ESI-MS).[13−15] ^{27}Al NMR chiefly distinguishes between different aluminum coordination states. However, it falls short in differentiating aluminum polyoxocations with similar coordination environments and fails to detect highly unsymmetrical pentacoordinate aluminum

Received: July 18, 2024
Revised: August 28, 2024
Accepted: August 30, 2024
Published: September 13, 2024

https://doi.org/10.1021/acs.langmuir.4c02751
Langmuir 2024, 40, 20284−20293

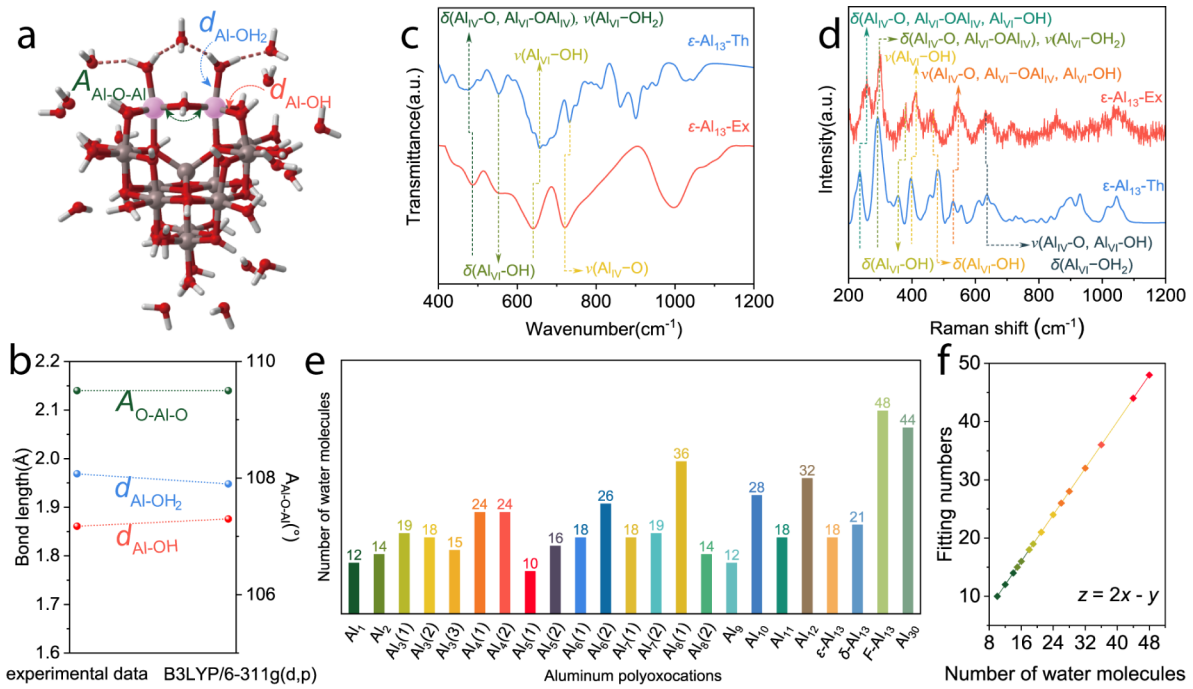

Figure 1. (a) The geometrical structure of ε-Al_{13}. (b) Comparison of the experimental and theoretical bond lengths and bond angles. The experimental and theoretical spectral characteristics of (c) infrared spectrum and (d) Raman spectrum of ε-Al_{13}. (e) Number of water molecules in the second hydration layer for the aluminum polyoxocations. (f) The linear scaling relationship for the number of water molecules in the secondary hydration layer.

species.[16] The ferron colorimetric method provides a rough classification of aluminum into three kinetic forms: Al_a, Al_b, and Al_c.[17] The ESI-MS technique's peak-matching procedure is inherently subjective, posing a challenge to validating results.[18] Conversely, infrared spectroscopy and Raman scattering are increasingly pivotal due to their capability to deliver distinctive "fingerprint" spectra, facilitating the identification of various species or molecules.[19] The integration of density functional theory (DFT) calculations with infrared and Raman spectroscopic data is gaining traction as a methodology to pinpoint aluminum clusters and explicate the principles guiding their transformations.[20] Nonetheless, the prevalent knowledge of spectral attributes of aluminum polyoxocations is primarily confined to aluminum monomers and the Keggin series in aqueous environments.[21] This creates a significant gap in knowledge regarding other possible aluminum polyoxocations that may be present during the transition process, particularly those in thermodynamically unstable states. This limitation encumbers a complete understanding of the characterization, morphological evolution, and controlled formation of aluminum polyoxocations. Consequently, investigating the spectral characteristics of aluminum polyoxocations via theoretical approaches is of prime importance in unraveling the structural evolution of these species within solutions.

In this article, we employed DFT calculations to model the spectral signatures of potential aluminum polyoxocations in aqueous environments. These spectral fingerprints encompass infrared and Raman spectra and ^{27}Al NMR chemical shifts. A thorough examination of the spectral features of various aluminum clusters is undertaken, with specific attention given to the utilization of spectral data in distinguishing these entities. At near-neutral and higher pH, the dominant multimeric aluminum complex in aqueous systems is the large polyoxocation, $[AlO_4Al_{12}(OH)_{24}(H_2O)_{12}]^{7+}$, which forms rapidly via Al^{3+} hydrolysis. This complex consists of a central tetrahedrally coordinated AlO_4 moiety, enveloped by a sheath of 12 edge-shared AlO_6 units arranged in four sets of three linked trimers. The most familiar form of this molecule is referred to as ε-Al_{13}.[22] This work endeavors to pinpoint critical intermediaries implicated in the transformation of aluminum monomers into ε-Al_{13} clusters, leveraging alterations in NMR resonances and concomitant Raman shifts induced by solutions varying in basicity. Furthermore, throughout this research, a putative conversion trajectory from Al_1 to ε-Al_{13} is postulated and predicated on the energetically optimized structures. The ultimate objective is to demystify the metamorphosis of diverse aluminum clusters in aqueous solutions, thereby furnishing a foundational reference for understanding such processes.

MATERIALS AND METHODS

Preparation of PACl Solutions. Polyaluminum chloride (PACl) solutions boasting a range of basicities (with basicity B set between 0.4 and 2.6, incremented by $\Delta B = 0.2$) were conducted through titration experiments. In a typical procedure, a 0.25 mol L^{-1} NaOH solution was incrementally added to 10 mL of 0.25 mol L^{-1} $AlCl_3$ solution maintained at a temperature of 80 °C until the intended B value was attained. Following each basicity increment, the mixture was stirred vigorously for one min, after which the pH was meticulously documented upon stabilization. Solid samples of PACl for ^{27}Al NMR and Raman spectral analysis were obtained through the freeze-drying of the specific solutions targeted in this study.[17]

Purification of the ε-Al_{13} Cluster. The synthesized PACl with a basicity (B) of 2.2 underwent a purification process using sulfate precipitation, followed by a chloride ion exchange method, to procure ε-Al_{13} salts of elevated purity. The initial

https://doi.org/10.1021/acs.langmuir.4c02751
Langmuir 2024, 40, 20284−20293

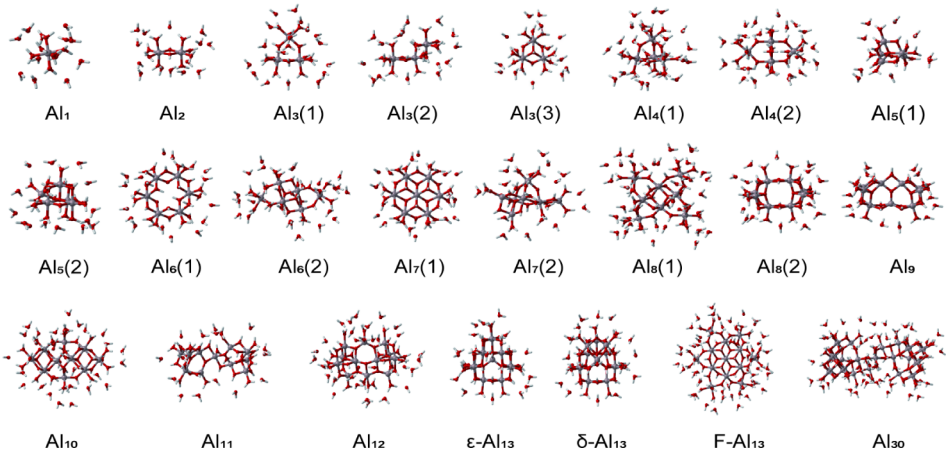

Figure 2. Optimized geometries of aluminum polyoxocations.

step involved a mixture of PACl with a Na_2SO_4 solution (0.1 M) under magnetic stirring, aiming for a targeted SO_4^{2-}/Al molar ratio of 1.0. After several days, crystals of Na-$(H_2O)_4[AlO_4Al_{12}(OH)_{24}(H_2O)_{12}](SO_4)_4{\cdot}10H_2O$, denoted as Al_{13}-$(SO_4)_p$, were formed. These Al_{13}-$(SO_4)_p$ crystals were then rinsed with deionized water and subsequently dried at 25 °C, preparing them for the ensuing metathesis reaction. The generation of the pure $Al_{13}-Cl_n$ solution was carried out through a Ba^{2+}/SO_4^{2-} metathesis reaction. Specifically, the ε-Al_{13} sulfate material was introduced into a 40 mL $BaCl_2$ solution and agitated for 180 min. The $Al_{13}-Cl_n$ solution was obtained by centrifugation and filtration of this mixture. The speciation of the resultant aluminum in the filtrate was ascertained by using liquid-state ^{27}Al NMR spectroscopy. Finally, the $Al_{13}-Cl_n$ solution was lyophilized, yielding the $Al_{13}-Cl_n$ solid, which was set for further solid-state ^{27}Al NMR and Raman spectral analysis.[23]

DFT Calculations. All the structural optimization and spectral characteristics calculations were conducted using Gaussian 16.[24] The SM-PCM approach was employed to account for explicit solvent effects by introducing a varying number of solvent water molecules with hydrogen bonds.[25] Meanwhile, the polarizable continuum model (PCM) was adopted to simulate bulk solvent effects.[26] The geometry optimization and frequency analysis of the aluminum polyoxocations were performed using the B3LYP/6-311G(d,p) method, with a frequency scaling factor of 0.9640 applied for frequency correction.[27,28] Notably, all of the structures of aluminum polyoxocations were initially preoptimized under gas-phase conditions before water molecules were added to simulate the solvent effects. The Raman spectrum was calculated using the B3LYP/6-311+G(d,p) theoretical level and further corrected with a frequency scaling factor of 0.9688.[29] The program Multiwfn was utilized to convert Raman activity values to Raman intensities.[30] Moreover, ^{27}Al NMR chemical shifts for all complexes were determined by the GIAO method at the Hartree−Fock/6-311+G(d,p) level.[31]

RESULTS AND DISCUSSION

Determination of the Solvent Structures of Aluminum Polyoxocations. *Exploration of Solvated Aluminum Polyoxocations.* The architecture of aluminum polyoxocations presents a confounding complexity. Thus, it is crucial to determine a universal rule for solvent water molecules within the secondary hydration stratum.[32] Recognizing the critical interaction between the clusters and the water molecules, we placed two water molecules following each water ligand, creating a hydrogen-bonded matrix. The ε-Al_{13} cluster has a four-membered ring structure consisting of two aluminum atoms and two oxygen atoms. The water ligands in the closest hydration layer are close enough and adequately oriented to form hydrogen bonds with a water molecule in the secondary hydration layer and with nearby water molecules in the four-membered ring. As shown in Figure 1a, this interaction culminates in the formation of an intricate "pentamer water molecule with quartet hydrogen bond" network configuration.

Our investigations continued with optimizing ε-Al_{13}, an essential aluminum species, followed by frequency computations. Drawing comparisons with empirical values, the architectural parameters depicted by our computational frameworks, involving bond lengths and angles, exhibit a remarkable congruence with actual measurements, as shown in Figure 1d.[33] Furthermore, the infrared and Raman spectral frequencies align closely with experimental findings, as depicted in Figure 1b,c.[34] Besides, the theoretical ^{27}Al NMR chemical shifts of $Al-O_4$ in ε-$A1_{13}$ and $Al(H_2O)_6^{3+}{\cdot}12H_2O$ are calculated to be 549.2 and 609.9 ppm, respectively, with their differential of 60.7 ppm nearing the experimental benchmark of 62.5 ppm.[35]

In light of these insights, we postulate that the infrared and Raman spectral attributes of aluminum polyoxocations could be inferred by appending solvent water molecules to each water ligand from the initial hydration shell to form dual hydrogen bonds. In conclusion, we proposed a predictive model for the number of water molecules needed in the secondary hydration layer (Figure 1e,f). The governing equation for this postulation is presented as $z = 2x - y$, where x signifies the aggregate of water molecules within the foremost solvation layer, while y represents the sum of water molecule dyads arrayed upon disparate aluminum atoms that are situated within sub-4 Å proximity.

Determination of the Solvanted Geometrical Structures. Our optimization of aluminum polyoxocation structures draws upon three principal sources of data:

> Crystal structures reputed to be viable in aqueous solutions are a foundational resource, as evidenced by reported species such as Al_1, Al_2, $Al_4(1)$, $Al_6(1)$, $Al_8(1)$, ε-Al_{13}, δ-Al_{13}, F-Al_{13}, and Al_{30}.[36−45]
>
> The framework structures of aluminum polyoxocations bound by organic ligands or alternative reagents, as

https://doi.org/10.1021/acs.langmuir.4c02751
Langmuir 2024, 40, 20284−20293

reported in the literature, provide a further basis. Examples include $Al_3(1)$, $Al_3(2)$, $Al_3(3)$, $Al_4(2)$, $Al_5(1)$, $Al_5(2)$, $Al_6(2)$, $Al_7(1)$, $Al_7(2)$, $Al_8(2)$, Al_9, Al_{10}, and Al_{11}.[46−55]

Structural analogues reported for gallium, an element similar to aluminum, provide a third source of information. The similarity in properties between aluminum and gallium suggests that gallium's structural data can inform aluminum analyses. Notably, gallium often replaces the central aluminum atom in $Al−O_4$ when studying the structural characteristics of Keggin-Al_{13}. This supports our choice of the reported Ga_{12} as a surrogate framework for Al_{12} optimization.[56]

Thus, we optimized a suite of aluminum polyoxocations ranging from monomeric to Al_{13} and encompassing Al_{30}, culminating in 23 distinct and stable structures. All corresponding molecular formulas are meticulously cataloged in Table S1, with visual structures presented in Figure 2. Additionally, these aluminum polyoxocations' solvent-associated structures have been optimized, with their stability corroborated through frequency calculations.

Theoretical IR, NMR, and Raman Spectra of Aluminum Polyoxocations. To delineate the structural transitions occurring during the hydrolysis of aluminum polyoxocations, we employed DFT calculations to predict the IR, Raman, and ^{27}Al NMR spectra to ascertain the presence of such species in aqueous environments. Noteworthily, the Al−O vibrational modes predominantly manifest at wavenumbers beneath 1200 cm^{-1}. Hence, the IR spectral analysis concentrated on computation-derived values spanning from 400 to 1200 cm^{-1}, while the Raman spectrum scrutiny was similarly focused on the calculated range of 200−1200 cm^{-1}. Due to diminished structural symmetry and the vibrational coupling with water molecules, the same Al−O vibrational modes are registered at multiple frequencies. Therefore, a higher density of calculated peaks than experimental findings has been shown.[57]

The calculated IR and Raman spectra of typical aluminum polyoxocations are illustrated in heat maps and complemented by the NMR spectra. The chemical shifts observed in aluminum polyoxocations can be broadly categorized into three distinct groups based on the coordination number that indicates the surrounding environment of the aluminum atoms (Figure 3). The chemical shifts for octahedrally coordinated (six-coordinated) aluminum atoms predominantly feature within the 0−20 ppm range. For atoms in a pentacoordinated state, the shifts typically lie between 30 and 40 ppm. Atoms with tetrahedral coordination (four-coordinated) exhibit shifts clustered in the 60−80 ppm region.[58] However, detecting pentacoordinate aluminum polyoxocations via liquid-state NMR spectroscopy is notably challenging. Primarily, it is attributed to their pronounced asymmetry within the coordination sphere.[31] When assessing primary aluminum polyoxocations, namely Al_1 through Al_4, the observed trend indicates that the chemical shifts move toward the lower field as the degree of oligomerization increases. The chemical shifts associated with linear $Al_3(2)$, ring-shaped $Al_3(1)$, and $Al_3(3)$, as well as two structurally distinct Al_4 clusters, exhibit significant similarities. Thus, it is a complex task to distinguish them via NMR spectroscopy.

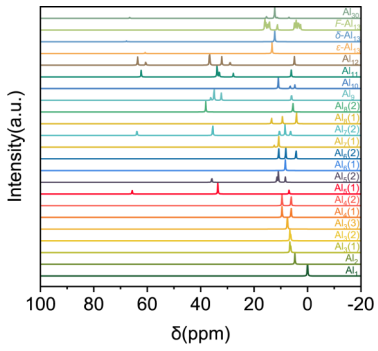

Figure 3. Simulated NMR spectra of aluminum polyoxocations.

The IR data illustrate that identical Al−O vibrational frequencies appear at various positions (Figure 4a); this, coupled with the similarity in structures across different aluminum polyoxocations, gives rise to similar vibrational frequencies. Consequently, the IR spectrum is characterized by broad spectral features.[59] This spectral breadth makes it challenging to pinpoint specific aluminum polyoxocation types within a composite system. Despite inconsistencies in the locations of peak intensities among diverse aluminum polyoxocations.

The Raman spectrum of aluminum polyoxocations shows a loss of Raman activity for certain Al−O vibrations (Figure 4b), resulting in distinct spectral signatures of different polyoxocations. These unique spectral features hold promise for subsequent analyses focusing on the structural evolution of aluminum polyoxocations as a function of increasing basicity. The Raman bands of $Al(H_2O)_6^{3+}$ at 502 and 393 cm^{-1} are representative of the $Al_{VI}−OH_2$ stretching ($\nu Al_{VI}−OH_2$) and bending ($\delta Al_{VI}−OH_2$) modes, respectively.[57] The spectrum of Al_2 is characterized by three consecutive peaks between 350 and 450 cm^{-1}, which serve as distinct markers for Al_2 polymer identification. Besides, the peaks at 428 cm^{-1}, 392 cm^{-1}, and 354 cm^{-1} correspond to $\nu Al_{VI}−OH$, $\nu Al_{VI}−OH_2$, and $\delta Al_{VI}−OH_2$, respectively. In the case of cyclic $Al_3(1)$, its Raman spectrum exhibits a band at 506 cm^{-1} due to the $\nu Al_{VI}−OH_2$ stretching vibration and a band at 377 cm^{-1} attributable to $\delta Al_{VI}−OH_2$. Conversely, the chain-like $Al_3(2)$ structure's spectrum is discernibly different, with a pronounced peak at 540 cm^{-1} ascribed to the $Al_{VI}−OH$ stretching vibration. The broad peaks between 350 and 380 cm^{-1} arise from the overlapping strong peaks at 351 and 376 cm^{-1}, which are ascribed to $\delta Al_{VI}−OH_2$ and $\delta Al_{VI}−OH$, respectively. The peak for $Al_3(3)$ at 392 cm^{-1} is likely due to $\delta Al_{VI}−OH_2$. Therefore, Raman spectra for the three differing Al_3 configurations are markedly distinct and can be separately identified.

Meanwhile, $Al_4(1)$ features significant $\delta Al_{VI}−OH_2$ vibrations at 406 cm^{-1}, and $Al_4(2)$ exhibits a notable $\delta Al_{VI}−OH_2$ vibration at 392 cm^{-1} and a $\delta Al_{VI}−OH$ vibration at 527 cm^{-1}. The prominent peak at 527 cm^{-1} facilitates discrimination between the two Al_4 clusters. The $Al_5(1)$ vibration modes at 365 cm^{-1} correspond to $\delta Al_V−OH_2$, while $Al_5(2)$'s most intense vibration at 341 cm^{-1} relates to $\delta Al_{VI}−OH$, with a secondary peak at 372 cm^{-1} originating from $\delta Al_{VI}−OH$. The vibrations for $Al_6(1)$ and $Al_6(2)$ at 567 and 556 cm^{-1}, respectively, are linked to $\nu Al_{VI}−OH$, with $Al_6(2)$ also showing a $\delta Al_{VI}−OH$ vibration at 587 cm^{-1}. The 616 cm^{-1} vibration in $Al_7(1)$ is due to $\nu Al_{VI}−OH_2$, whereas the irregular peak at 348 cm^{-1} in $Al_7(2)$ pertains to $\delta Al_{VI}−OH$. The 510 cm^{-1} peak in the $Al_8(1)$ spectrum is attributable to $\nu Al_{VI}−OH$. Besides, the $Al_8(2)$'s most intense vibration at 340 cm^{-1} is associated with

https://doi.org/10.1021/acs.langmuir.4c02751
Langmuir 2024, 40, 20284−20293

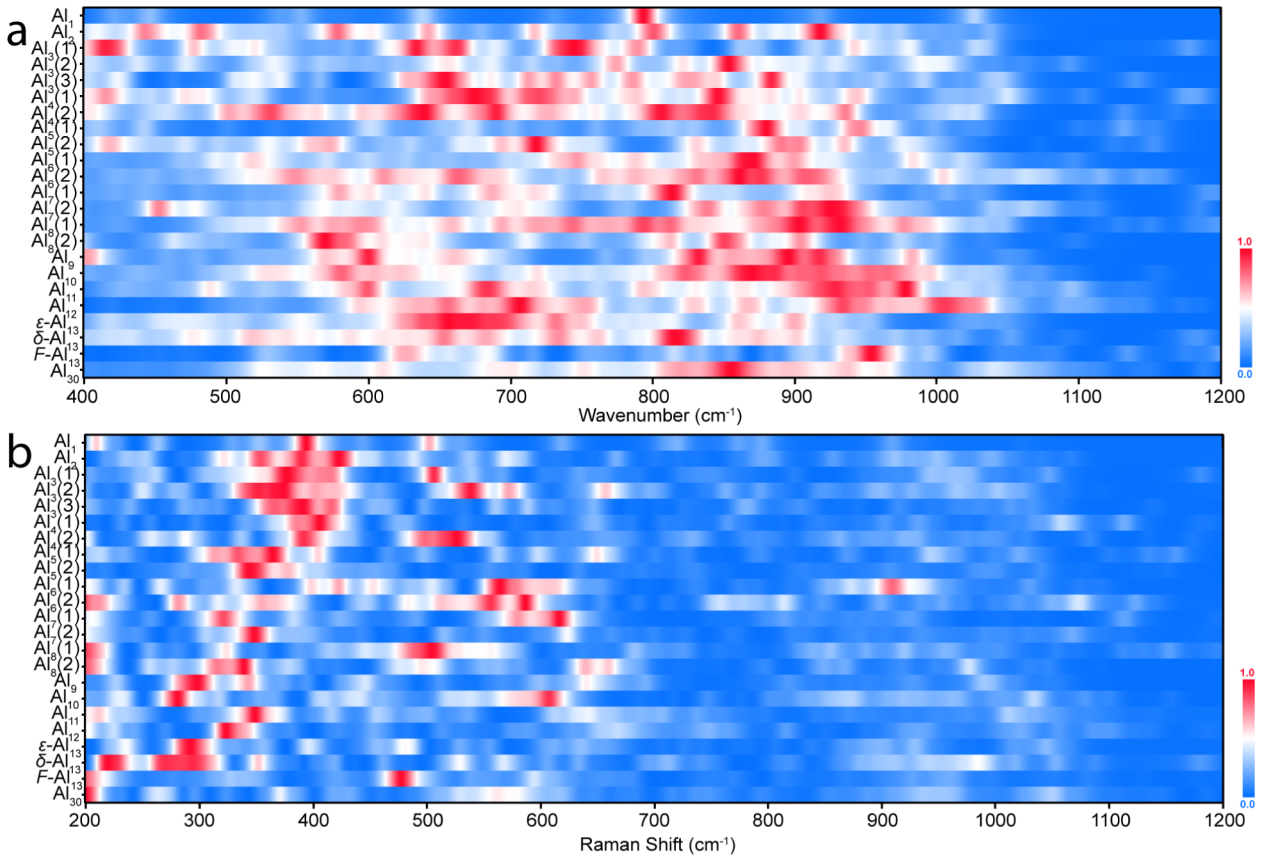

Figure 4. Heat maps for the spectral characteristics of (a) simulated infrared and (b) simulated Raman spectra.

νAl_V-OH_2, with a marginally less intense peak at 640 cm^{-1} attributed to νAl_V-OH. In addition, Al_9 features a peak at 301 cm^{-1} ascribed to δAl_V-OH and a weaker peak at 344 cm^{-1} linked to νAl_V-OH_2. The Al_{10} peaks at 282 and 608 cm^{-1} are assigned to $\delta Al_{VI}-OH$ and $\nu Al_{VI}-OH$, respectively. Both the intense peak at 348 cm^{-1} and the significant secondary peak at 209 cm^{-1} in Al_{11} indicate δAl_V-OH vibrations. The 322 cm^{-1} mode in Al_{12} is associated with δAl_V-OH.

For well-known ε-Al_{13}, its characteristic peak at 297 cm^{-1} is allocated to $\delta Al_{VI}-OH$. On the other hand, its isomer δ-Al_{13} shows similar modes at 295 cm^{-1}, belonging to $\delta Al_{VI}-OH$, with a matching intensity peak at 219 cm^{-1} ascribed to the same vibration.[34] The dual pronounced peaks between 200 and 300 cm^{-1} serve as identifiers for δ-Al_{13}. Notably, Al_9 shows the strongest peak around 300 cm^{-1}, similar to those of both Al_{13} clusters. However, it distinguishes itself by the discernible presence of a less pronounced peak at 344 cm^{-1}. The peak at 477 cm^{-1} in F-Al_{13} primarily relates to $\nu Al_{VI}-OH$, whereas the strongest vibration of Al_{30} at 203 cm^{-1} originates from $\delta Al_{VI}-OH$.[60] The characteristic peaks for the triad of clusters, $Al_5(2)$, $Al_7(2)$, and Al_{11}, are all found near 345 cm^{-1}. However, due to $Al_5(2)$'s significant subpeak at 372 cm^{-1}, it presents a broad spectrum characteristic in the 340−370 cm^{-1} range. Similarly, Al_{11}'s subpeak at 211 cm^{-1} is indicative. These subpeaks are valuable for distinguishing between the three cluster types.

To encapsulate the theoretical spectral analysis findings, we conclude that Raman spectroscopy presents a viable method for differentiating aluminum polyoxocations. Computational data reveal that the majority of robust vibrational signatures for these entities clusters within the 400−600 cm^{-1} spectrum. These are predominantly attributable to $Al-OX_n$ stretching vibrations, with a few modes corresponding to $Al_{VI}-OH_2$ bending vibrations. Concurrently, the prominent vibrational modes within the 200−400 cm^{-1} region are primarily related to $Al-OX_n$ bending vibrations, albeit with a limited number indicative of Al_V-OH_2 stretching vibrations.

Structural Evolution of Aluminum Polyoxocations along with Basicity. Delving into the structural metamorphosis of aluminum polyoxocations prompted by variances in basicity, our attention shifted toward the spectroscopic analysis of $AlCl_3$ across a spectrum of basic environments. Since aluminum monomers and ε-Al_{13} are the predominant aluminum−oxygen clusters present in solutions, they were selected for comparative analysis.[61] The pure $AlCl_3$ and ε-Al_{13} are employed as benchmarks. ^{27}Al NMR spectra of the aluminate solutions are delineated by resonances consistent with $Al(H_2O)_6^{3+}$ at 0 ppm and ε-Al_{13} species at 62.5 ppm. Meanwhile, $Al(OH)_4^-$ solutions were added as an internal standard at 80 ppm.[62] According to ^{27}Al NMR spectra (Figure 5), the categorization of aluminum polyoxocations within the solution yielded three distinct entities: Al_1 at 0 ppm, ε-Al_{13} at 62.5 ppm, and a group of six-coordinated aluminum species spanning the 0−10 ppm spectral region within the basicity range of 0.4−1.4. These show good agreement with the simulated ^{27}Al NMR, especially for Al_1 (0 ppm) and ε-Al_{13} (60.7 ppm). According to theoretical simulation (Figure 3), the NMR peaks of several aluminum polyoxocations fall within this region, including Al_2, $Al_3(1)$, $Al_3(2)$, $Al_4(1)$, $Al_4(2)$, $Al_6(1)$, $Al_8(2)$, Al_9, F-Al_{13} or combinations thereof. Given that most aluminum polyoxocations contain hexacoordinated aluminum atoms, leading to similar chemical shifts, NMR

https://doi.org/10.1021/acs.langmuir.4c02751
Langmuir 2024, 40, 20284−20293

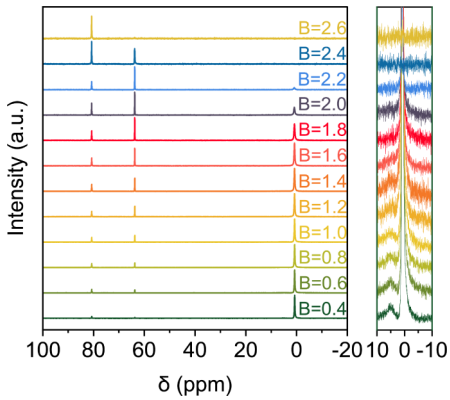

Figure 5. ^{27}Al NMR experimental spectra of the PACl solution under different alkalinity conditions.

spectra alone do not allow for precise identification of specific aluminum species.

The infrared spectra as cohesive entities exhibit features indicative of a broad spectrum profile (Figure 6a). In the basicity range of 0.4−1.2, the spectra predominantly reflect $AlCl_3$'s infrared peaks, suggesting the preeminence of aluminum monomers within the solution during this basicity interval.[63] As the basicity reaches a value of 1.4, we begin observing the emergence of vibrating signatures typical of ε-Al_{13}, followed by a subsequent amplification of its characteristic peaks.[64] The divergence in the Raman spectra becomes apparent at a basicity threshold of 2.0 (Figure 6b). At lower levels of basicity, the spectra exhibit the characteristic features of Al_1. As the basicity increases, there is a transition toward ε-Al_{13} spectral features. In contrast to the broader band characteristics of infrared spectra, Raman spectral peaks display a markedly higher resolution, conferring enhanced sensitivity to detect subtle peak displacements as a function of solution basicity. This particular clarity revealed by Raman spectroscopy endows us with the potential to conduct a more granulated analysis of aluminum cluster transformation within aqueous solutions.

With a motive to streamline observation, the peak positions of the Raman spectra were extracted for a more detailed analysis of their positional variations. These peak shifts notably correspond to the fraction of Al_m in relation to the total aluminum concentration (Al_T), as evidenced in Figure 7a. A peak in the ratio Al_m/Al_T is witnessed at a basicity of 0.6, showcasing a maximal influence on the peak displacement under this specific basicity.

As the ε-Al_{13} content ascends within the system, any alteration in shift trends is postulated to originate from emergent species, precluding the peak influence exerted by ε-Al_{13}. An explicit shift denotes that at B = 0.4, peaks at 561 and 595 cm^{-1} endure a slight red shift and reach B = 0.6, followed by a blue shift. It might be attributable to the transient inflation and subsequent deflation of Al_m levels. Raman spectra of the postulated species were compared (Figure 7b), revealing that only the shift induced by $Al_3(1)$ aligned with the observed patterns. The principal discrepancy between Raman peaks of Al_1 and $Al_3(1)$ is prominently observed at 600 cm^{-1}, aligning with the empirical spectrum.[65] The characteristic Raman peak of $Al_3(1)$ at 506 cm^{-1} closely resembles that of Al_1 at 502 cm^{-1}, elucidating why the experimental peak at 521 cm^{-1} displays a negligible shift. This reflects the putative existence of an intermediary, $Al_3(1)$, which mediates the transition from an aluminum monomer to ε-Al_{13}.

Conversely, significant shifts in tendencies are noted within the basicity range of 0.8−1.8. This suggests a phase transition among the predominant mixed species present, although low-symmetry entities remain undetectable by ^{27}Al NMR measurements. Moreover, the intricacies of the infrared Raman spectra preclude definitive species transition identification within this interval. This exposition emphasizes the need for further investigative efforts into the transformation pathway of

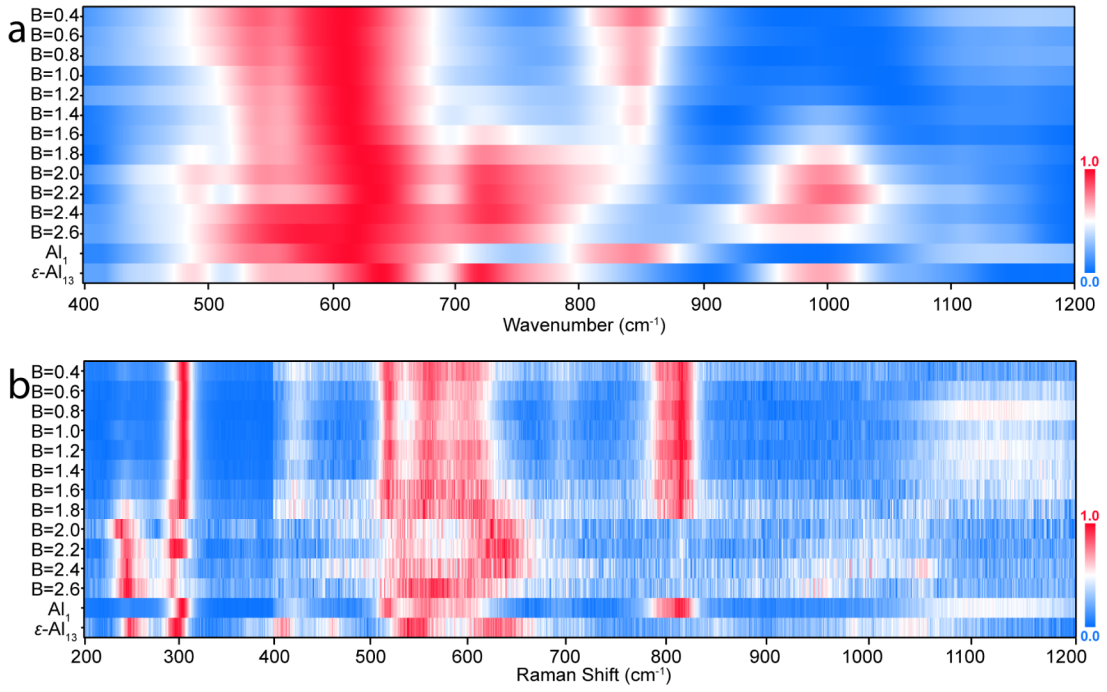

Figure 6. Heat maps of Al_1−Al_{13} and Al_{30} under different alkalinity conditions: (a) experimental IR spectra and (b) experimental Raman spectra.

https://doi.org/10.1021/acs.langmuir.4c02751
Langmuir 2024, 40, 20284−20293

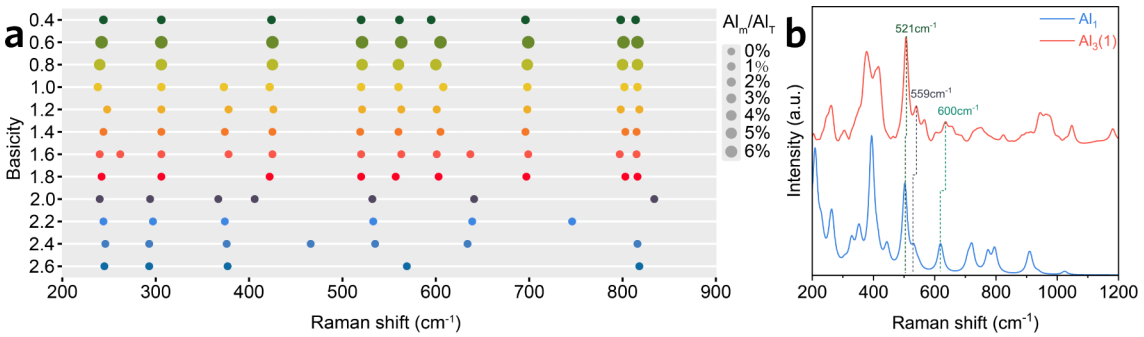

Figure 7. (a) Schematic diagram related to the Al_m/Al_T ratio and Raman peak shift. (b) Schematic diagram comparing the theoretical Raman spectra of Al_1 and $Al_3(1)$.

aluminum clusters. However, this also hints at the numerous unresolved questions within this domain.

Speculation on the Evolution of Al_1 to ε-Al_{13}. The formation of ε-Al_{13} appears to occur solely through $Al_3(1)$ and Al_1, without involving other intermediate species. This proposal faces criticism due to the distinctive vibrational mode of Al_{IV}−OAl_{VI}. Examination of all optimized structural configurations suggests that $Al_3(1)$ undergoes a transformation in the solution, converting initially into another variant known as $Al_3(3)$.[66] As depicted in Figure 8, this form subsequently

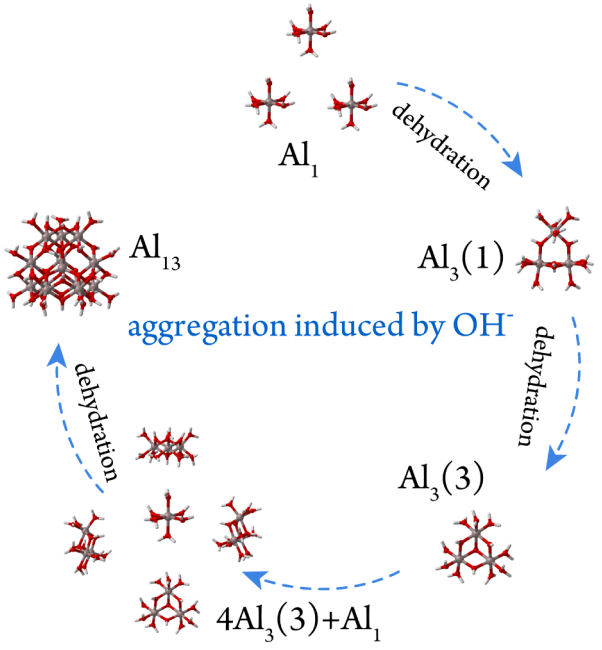

Figure 8. Schematic diagram of the evolution of Al_1 to ε-Al_{13}.

combines with a deprotonated, plastically deformed aluminum monomer. Ultimately, this process leads to the formation of ε-Al_{13}.[67] While confirmatory evidence remains elusive, the isolated $Al_8(2)$ configuration intimates the potential for polymerization events involving two $Al_3(3)$ units. Furthermore, μ_3-OH species are known for their proton-dissociative tendencies. They can easily combine with aluminum monomers, thereby providing the necessary structure for the formation of ε-Al_{13}.

CONCLUSIONS

In conclusion, we employed density functional theory to predict the infrared spectra, Raman spectra, and ^{27}Al NMR spectra of the possible aluminum polyoxocations in aqueous solutions, creating a comprehensive database. We aim to furnish a robust reference point for the analytical discernment and recognition of aluminum clusters in such environments. ^{27}Al NMR characterizations under varying basicities have separated the aluminum oxygen cluster population into three distinct factions: aluminum monomers, ε-Al_{13} entities, and six-coordinated aluminum species. Inferences drawn from NMR shifts and Raman spectral peak shifts propose the involvement of $Al_3(1)$, indicating its presence during the aluminum monomer's transformation into ε-Al_{13}. Building upon these findings, we have articulated a potential formation avenue for ε-Al_{13} via the transition of $Al_3(1)$ into $Al_3(3)$, which subsequently amalgamates with structurally altered Al_1. We anticipate that these insights might serve as pivotal guides in elucidating the metamorphic pathways of aluminum clusters within aqueous media.

ASSOCIATED CONTENT

Data Availability Statement

The data that support the findings of this study are available from the corresponding author upon reasonable request.

Supporting Information

The Supporting Information is available free of charge at https://pubs.acs.org/doi/10.1021/acs.langmuir.4c02751.

Vibration modes of aluminum polyoxocations, structural formula, and corresponding structural coordinates (PDF)

AUTHOR INFORMATION

Corresponding Authors

Yuguo Xia − *National Engineering Research Center for Colloidal Materials, School of Chemistry and Chemical Engineering, Shandong University, Jinan, Shandong 250100, China;* orcid.org/0000-0002-0405-3439; Email: xyg@sdu.edu.cn

Dairong Chen − *National Engineering Research Center for Colloidal Materials, School of Chemistry and Chemical Engineering, Shandong University, Jinan, Shandong 250100, China;* orcid.org/0000-0001-6961-9328; Email: cdr@sdu.edu.cn

https://doi.org/10.1021/acs.langmuir.4c02751
Langmuir 2024, 40, 20284−20293

Authors

Qi Zhao − *National Engineering Research Center for Colloidal Materials, School of Chemistry and Chemical Engineering, Shandong University, Jinan, Shandong 250100, China*

Minjuan Zhao − *National Engineering Research Center for Colloidal Materials, School of Chemistry and Chemical Engineering, Shandong University, Jinan, Shandong 250100, China*

Xiuling Jiao − *National Engineering Research Center for Colloidal Materials, School of Chemistry and Chemical Engineering, Shandong University, Jinan, Shandong 250100, China;* orcid.org/0000-0002-4358-7396

Complete contact information is available at: https://pubs.acs.org/10.1021/acs.langmuir.4c02751

Author Contributions

Y.X. supervised the project. Q.Z. performed all the simulations and elemental data analysis. M.Z. was responsible for the synthesis of experimental samples. X.J. and D.C. discussed the theoretical results and provided the fund support. Q.Z. and Y.X. wrote this manuscript, and all authors contributed to the overall scientific interpretation and revised this paper.

Funding

This work was financially supported by the Young Scholars Program of Shandong University, the National Natural Science Foundation of China (grant 22275116), and the Natural Science Foundation of Shandong Province (Major Basic Research) project (grant ZR2023ZD19).

Notes

The authors declare no competing financial interest.

■ ACKNOWLEDGMENTS

The authors acknowledge Beijing PARATERA Tech Co., Ltd. for providing HPC resources that have contributed to the research results reported in this paper.

■ REFERENCES

(1) Botté, A.; Zaidi, M.; Guery, J.; Fichet, D.; Leignel, V. Aluminium in aquatic environments: Abundance and ecotoxicological impacts. *Aquat. Ecol.* **2022**, *56* (3), 751−773.

(2) Mullapudi, K.; Murari, N. M.; Mansergh, R. H.; Keszler, D. A.; Conley, J. F., Jr Area-selective aerosol jet fog deposition: Advancing large-area and sustainable facbrication. *J. Vac. Sci. Technol., A* **2021**, *39* (1), 013407.

(3) Huang, B.; Li, C.; Zhang, Y.; Ding, W.; Yang, M.; Yang, Y.; Zhai, H.; Xu, X.; Wang, D.; Debnath, S.; Jamil, M.; Li, H. N.; Ali, H. M.; Gupta, M. K.; Said, Z. Advances in fabrication of ceramic corundum abrasives based on sol-gel process. *Chin. J. Aeronaut.* **2021**, *34* (6), 1−17.

(4) Moshkovitz, M. Y.; Paz, D.; Magdassi, S. 3D Printing Transparent γ-Alumina Porous Structures Based on Photopolymerizable Sol-Gel Inks. *Adv. Mater. Technol.* **2023**, *8* (23), 2300123.

(5) Zhang, W.; Tang, M.; Li, D.; Yang, P.; Xu, S.; Wang, D. Effects of alkalinity on interaction between EPS and hydroxy-aluminum with different speciation in wastewater sludge conditioning with aluminum based inorganic polymer flocculant. *J. Environ. Sci.* **2021**, *100*, 257−268.

(6) Liu, L.; Lu, S.; An, G.; Yang, B.; Zhao, X.; Wu, D.; He, H.; Wang, D. Historical development of Al_{30} highlighting the unique characteristics and application in water treatment: A review. *Coord. Chem. Rev.* **2022**, *473*, 214807.

(7) Casey, W. H. Large Aqueous Aluminum Hydroxide Molecules. *Chem. Rev.* **2006**, *106* (1), 1−16.

(8) Bi, S.; Wang, C.; Cao, Q.; Zhang, C. Studies on the mechanism of hydrolysis and polymerization of aluminum salts in aqueous solution: Correlations between the "Core-links" model and "Cage-like" Keggin-Al_{13} model. *Coord. Chem. Rev.* **2004**, *248* (5), 441−455.

(9) Lukić, M. J.; Wiedenbeck, E.; Reiner, H.; Gebauer, D. Chemical trigger toward phase separation in the aqueous Al(III) system revealed. *Sci. Adv.* **2020**, *6* (23), No. eaba6878.

(10) Swaddle, T. W.; Rosenqvist, J.; Yu, P.; Bylaska, E.; Phillips, B. L.; Casey, W. H. Kinetic Evidence for Five-Coordination in $AlOH(aq)^{2+}$ Ion. *Science* **2005**, *308* (5727), 1450−1453.

(11) Brunson, K. G.; Colla, C. A.; Oliveri, A. F.; Pan, L.; Casey, W. H. A conspicuous ^{27}Al-NMR signal at 72 ppm during isomerization of Keggin Al_{13} ions. *Inorg. Chim. Acta* **2021**, *514*, 120014.

(12) Bi, Z.; Feng, C.; Wang, D.; Ge, X.; Tang, H. Transformation of planar Mögel Al_{13} to epsilon Keggin Al_{13} in dissolution process. *Colloids Surf., A* **2012**, *407*, 91−98.

(13) Graham, T. R.; Chun, J.; Schenter, G. K.; Zhang, X.; Clark, S. B.; Pearce, C. I.; Rosso, K. M. ^{27}Al NMR diffusometry of Al_{13} Keggin nanoclusters. *Magn. Reson. Chem.* **2022**, *60* (2), 226−238.

(14) Tian, C.; Feng, C.; Wang, Q. The identification of Al nanoclusters by electrospray ionization mass spectrometry (ESI-MS). *Sci. Total Environ.* **2021**, *754*, 142154.

(15) Wang, X.; Xu, H.; Wang, D. Mechanism of fluoride removal by $AlCl_3$ and Al_{13}: The role of aluminum speciation. *J. Hazard. Mater.* **2020**, *398*, 122987.

(16) An, G.; Yue, Y.; Wang, P.; Liu, L.; Demissie, H.; Jiao, R.; Wang, D. Deprotonation and aggregation of Al_{13} under alkaline titration: A simulating study related to coagulation process. *Water Res.* **2021**, *203*, 117562.

(17) Chen, Y.; Matsui, Y.; Sato, T.; Shirasaki, N.; Matsushita, T. Overlooked effect of ordinary inorganic ions on polyaluminum-chloride coagulation treatment. *Water Res.* **2023**, *235*, 119909.

(18) Tian, C.; Wu, Y.; Wei, M.; Feng, C. A novel understanding of residual nano-Al_{13} formation and degradation during coagulation and flocculation: A proof based on ESI-TOF-MS. *Environ. Sci.: Nano* **2018**, *5* (11), 2712−2721.

(19) Fang, C.; Tang, L. Mapping Structural Dynamics of Proteins with Femtosecond Stimulated Raman Spectroscopy. *Annu. Rev. Phys. Chem.* **2020**, *71*, 239−265.

(20) Wang, W.; Liu, W.; Chang, I.-Y.; Wills, L. A.; Zakharov, L. N.; Boettcher, S. W.; Cheong, P. H.-Y.; Fang, C.; Keszler, D. A. Electrolytic synthesis of aqueous aluminum nanoclusters and in situ characterization by femtosecond Raman spectroscopy and computations. *Proc. Natl. Acad. Sci. U. S. A.* **2013**, *110* (46), 18397−18401.

(21) Wen, K.; Zhu, J.; Chen, H.; Ma, L.; Liu, H.; Zhu, R.; Xi, Y.; He, H. Arrangement Models of Keggin-Al_{30} and Keggin-Al_{13} in the Interlayer of Montmorillonite and the Impacts of Pillaring on Surface Acidity: A Comparative Study on Catalytic Oxidation of Toluene. *Langmuir* **2019**, *35* (2), 382−390.

(22) Armstrong, C. R.; Casey, W. H.; Navrotsky, A. Energetics of Al_{13} Keggin cluster compounds. *Proc. Natl. Acad. Sci. U. S. A.* **2011**, *108* (36), 14775−14779.

(23) An, G.; Yue, Y.; Yang, L.; Demissie, H.; Jiao, R.; Xi, J.; Wang, D. Decomposition of Al_{13} promoted by salicylic acid under acidic condition: Mechanism study by differential mass spectrometry method and DFT calculation. *J. Environ. Sci.* **2023**, *126*, 423−433.

(24) Frisch, M. J.; Trucks, G. W.; Schlegel, H. B.; Scuseria, G. E.; Robb, M. A.; Cheeseman, J. R.; Scalmani, G.; Barone, V.; Petersson, G. A.; Nakatsuji, H., et al. *Gaussian 16 Rev. C.01*, Gaussian Inc. Wallingford, CT, 2016.

(25) Becke, A. D. Density-functional thermochemistry. III. The role of exact exchange. *J. Chem. Phys.* **1993**, *98* (7), 5648−5652.

(26) Tomasi, J.; Mennucci, B.; Cammi, R. Quantum Mechanical Continuum Solvation Models. *Chem. Rev.* **2005**, *105* (8), 2999−3094.

(27) Merrick, J. P.; Moran, D.; Radom, L. An Evaluation of Harmonic Vibrational Frequency Scale Factors. *J. Phys. Chem. A* **2007**, *111* (45), 11683−11700.

(28) Kashinski, D. O.; Chase, G. M.; Nelson, R. G.; Di Nallo, O. E.; Scales, A. N.; VanderLey, D. L.; Byrd, E. F. C. Harmonic Vibrational

Frequencies: Approximate Global Scaling Factors for TPSS, M06, and M11 Functional Families Using Several Common Basis Sets. *J. Phys. Chem. A* **2017**, *121* (11), 2265−2273.
(29) Wolinski, K.; Hinton, J. F.; Pulay, P. Efficient implementation of the gauge-independent atomic orbital method for NMR chemical shift calculations. *J. Am. Chem. Soc.* **1990**, *112* (23), 8251−8260.
(30) Lu, T.; Chen, F. Multiwfn: A multifunctional wavefunction analyzer. *J. Comput. Chem.* **2012**, *33* (5), 580−592.
(31) Dong, S.; Shi, W.; Zhang, J.; Bi, S. ^{27}Al NMR Chemical Shifts and Relative Stabilities of Aqueous Monomeric Al^{3+} Hydrolytic Species with Different Coordination Structures. *ACS Earth Space Chem.* **2019**, *3* (7), 1353−1361.
(32) Yang, W.; Qian, Z.; Lu, B.; Zhang, J.; Bi, S. Density functional theory study and kinetic analysis of the formation mechanism of $Al_{30}O_8(OH)_{56}(H_2O)_{26}^{18+}$ (Al_{30}) in aqueous solution. *Geochim. Cosmochim. Acta* **2010**, *74* (4), 1220−1229.
(33) Qian, Z.; Feng, H.; Yang, W.; Bi, S. Theoretical Investigation of Water Exchange on the Nanometer-Sized Polyoxocation $AlO_4Al_{12}(OH)_{24}(H_2O)_{12}^{7+}$ (Keggin-Al_{13}) in Aqueous Solution. *J. Am. Chem. Soc.* **2008**, *130* (44), 14402−14403.
(34) Li, N.; Hu, C.; Fu, X.; Xu, X.; Liu, R.; Liu, H.; Qu, J. Identification of Al_{13} on the Colloid Surface Using Surface-Enhanced Raman Spectroscopy. *Environ. Sci. Technol.* **2017**, *51* (5), 2899−2906.
(35) Allouche, L.; Taulelle, F. Conversion of Al_{13} Keggin ε into Al_{30}: A reaction controlled by aluminum monomers. *Inorg. Chem. Commun.* **2003**, *6* (9), 1167−1170.
(36) Berger, S.; Nolde, J.; Yüksel, T.; Tremel, W.; Mondeshki, M. ^{27}Al NMR Study of the pH Dependent Hydrolysis Products of $Al_2(SO_4)_3$ in Different Physiological Media. *Molecules* **2018**, *23* (4), 808.
(37) Cao, X.; Chen, M.; Wang, Y.; Shen, S.; Zhang, Z.; Li, B.; Sun, B. Al_{30} polycation pillared montmorillonite preparation and phosphate adsorption removal from water. *Surf. Interfaces* **2022**, *29*, 101780.
(38) Mauro, D.; Biagioni, C.; Sejkora, J.; Dolníček, Z.; Škoda, R. Batoniite, [Al8(OH)14(H2O)18](SO4)5 · 5H2O, a new mineral with the [Al8(OH)14(H2O)18]10+ polyoxocation from the Cetine di Cotorniano Mine, Tuscany, Italy. *Eur. J. Mineral.* **2023**, *35* (5), 703−714.
(39) Sun, Z.; Wang, H.; Feng, H.; Zhang, Y.; Du, S. Crystal Structure of $[Al_4(OH)_6(H_2O)_{12}][Al(H_2O)_6]_2Br_{12}$: A New Polyaluminum Compound. *Inorg. Chem.* **2011**, *50* (19), 9238−9242.
(40) Zhou, W.; Ogiwara, N.; Weng, Z.; Tamai, N.; Zhao, C.; Yan, L.-K.; Uchida, S. Isomeric effects on the acidity of Al_{13} Keggin clusters in porous ionic crystals. *Chem. Commun.* **2021**, *57* (71), 8893−8896.
(41) Rosen, A. Q.; Salpino, V.; Johnson, D. W. Observation of alumina nanoparticles generated from aqueous solutions of a "flat" aluminum-13 cluster. *Chem. Commun.* **2023**, *59* (83), 12483−12486.
(42) Smirnov, P. R.; Grechin, O. V. Structure of the Nearest Environment of Ions in Aqueous Solutions of Aluminum Chloride According to X-ray Diffraction. *Russ. J. Inorg. Chem.* **2018**, *63* (9), 1251−1255.
(43) Ivanova, Y.; Zhuzhgov, A.; Isupova, L. Synthesis of aluminum-copper catalysts based on product of centrifugal thermal activation of gibbsite and their activity in selective oxidation of ammonia. *Inorg. Chem. Commun.* **2024**, *162*, 112287.
(44) Jin, X.; Liao, R.; Zhang, T.; Li, H. Theoretical insights into the dimerization mechanism of aluminum species at two different pH conditions. *Inorg. Chim. Acta* **2021**, *520*, 120311.
(45) Shohel, M.; Smith, J. A.; Carolan, M. A.; Forbes, T. Z. Thermal Aging of Heteroatom-Substituted Keggin-Type Aluminum Oxo Polycation Solutions: Aggregation Behavior and Impacts on Humic Acid and Turbidity Removal. *ACS ES&T Water* **2022**, *2* (1), 22−31.
(46) Nachtigall, O.; Hirsch, T.; Spandl, J. Alcoholysis of $Al_2(OtBu)_6$ − Synthesis and Crystal Structure of $Al_9O_3(OEt)_{21}$. *Z. Anorg. Allg. Chem.* **2018**, *644* (1), 2−5.
(47) Dimitrov, A.; Koch, J.; Troyanov, S. I.; Kemnitz, E. Aluminum Alkoxide Fluorides Involved in the Sol-Gel Synthesis of Nanoscopic AlF_3. *Eur. J. Inorg. Chem.* **2009**, *2009* (35), 5299−5301.
(48) Butcher, R. J.; Purdy, A. P. The crystal structure of the decaaluminum alkoxide cluster $Al_{10}O4(OH)_8L_{14}$ (L = 1,1,1,3,3,3-hexafluoropropan-2-olate). *Acta Crystallogr. E: Crystallogr. Commun.* **2021**, *77* (2), 79−82.
(49) Xu, H.-B.; Chen, X.-M.; Zhang, Q.-S.; Zhang, L.-Y.; Chen, Z.-N. Fluoride-enhanced lanthanide luminescence and white-light emitting in multifunctional Al_3Ln_2 (Ln = Nd, Eu, Yb) hetero-pentanuclear complexes. *Chem. Commun.* **2009**, *47*, 7318−7320.
(50) Roy, M. M. D.; Omaña, A. A.; Wilson, A. S. S.; Hill, M. S.; Aldridge, S.; Rivard, E. Molecular Main Group Metal Hydrides. *Chem. Rev.* **2021**, *121* (20), 12784−12965.
(51) König, R.; Scholz, G.; Veiczi, M.; Jäger, C.; Troyanov, S. I.; Kemnitz, E. New crystalline aluminum alkoxide oxide fluorides: Evidence of the mechanism of the fluorolytic sol−gel reaction. *Dalton Trans.* **2011**, *40* (34), 8701−8710.
(52) Starikova, Z. A.; Kessler, V. G.; Turova, N. Y.; Tcheboukov, D. E.; Suslova, E. V.; Seisenbaeva, G. A.; Yanovsky, A. I. New polynuclear aluminium oxoalkoxides: Molecular structures of $Al_{11}(\mu_4\text{-}O)_2(\mu_3\text{-}O)_2(\mu\text{-}O)_2(\mu\text{-}OPrn)_{10}(\mu\text{-}OPri)_2(\mu\text{-}ROH)_2(OPri)_8(OR)$, R = Prn,i and $Al_5Mg_4(\mu_4\text{-}O)_2(\mu_3\text{-}O)(\mu\text{-}OH)_3(\mu\text{-}OPri)_8(\mu,\eta_2\text{-}acac)_4(\eta_2\text{-}acac)_2$. *Polyhedron* **2004**, *23* (1), 109−114.
(53) Carmalt, C. J.; Mileham, J. D.; White, A. J. P.; Williams, D. J. Pentanuclear alkoxyaluminium hydrides. *New J. Chem.* **2002**, *26* (7), 902−905.
(54) Fairley, M.; Unruh, D. K.; Abeysinghe, S.; Forbes, T. Z. Synthesis and Structural Characterization of Heterometallic Thorium Aluminum Polynuclear Molecular Clusters. *Inorg. Chem.* **2012**, *51* (17), 9491−9498.
(55) Zhang, X.-Z.; Wang, X.-F.; Fang, W.-H.; Zhang, J. Synthesis, Structures, and Fluorescence Properties of Dimeric Aluminum Oxo Clusters. *Inorg. Chem.* **2021**, *60* (10), 7089−7093.
(56) Suslova, E. V.; Kessler, V. G.; Gohil, S.; Turova, N. Y. Oxoethoxide Chlorides Representatives of Oligonuclear Alkoxide Complexes of Gallium: Penta- and Dodecanuclear Molecules. *Eur. J. Inorg. Chem.* **2007**, *2007* (33), 5182−5188.
(57) Lu, B.-M.; Jin, X.-Y.; Tang, J.; Bi, S.-P. DFT studies of Al-O Raman vibrational frequencies for aquated aluminium species. *J. Mol. Struct.* **2010**, *982* (1), 9−15.
(58) Chandran, C. V.; Kirschhock, C. E. A.; Radhakrishnan, S.; Taulelle, F.; Martens, J. A.; Breynaert, E. Alumina: Discriminative analysis using 3D correlation of solid-state NMR parameters. *Chem. Soc. Rev.* **2019**, *48* (1), 134−156.
(59) Mink, J.; Németh, C.; Hajba, L.; Sandström, M.; Goggin, P. L. Infrared and Raman spectroscopic and theoretical studies of hexaaqua metal ions in aqueous solution. *J. Mol. Struct.* **2003**, *661−662*, 141−151.
(60) Jackson, M. N., Jr; Wills, L. A.; Chang, I. Y.; Carnes, M. E.; Scatena, L. F.; Cheong, P. H.-Y.; Johnson, D. W. Identifying Nanoscale M_{13} Clusters in the Solid State and Aqueous Solution: Vibrational Spectroscopy and Theoretical Studies. *Inorg. Chem.* **2013**, *52* (10), 6187−6192.
(61) Tang, H.; Xiao, F.; Wang, D. Speciation, stability, and coagulation mechanisms of hydroxyl aluminum clusters formed by PACl and alum: A critical review. *Adv. Colloid Interface Sci.* **2015**, *226*, 78−85.
(62) Kanzaki, M. Ab Initio ^{27}Al NMR Chemical Shift Calculation for the Clusters of $Al(OH)_4^-$, $Al(OH)_5^{2-}$and $Al(OH)_6^{3-}$. *J. Ceram. Soc. Jpn.* **1997**, *105* (1217), 91−92.
(63) Adams, D. M.; Hills, D. J. Single-crystal Raman and infrared study of aluminium trichloride hexa-hydrate. *J. Chem. Soc., Dalton Trans.* **1978**, *7*, 782−788.
(64) Wang, D.; Wang, S.; Huang, C.; Chow, C. W. K. Hydrolyzed Al(III) clusters: Speciation stability of nano-Al_{13}. *J. Environ. Sci.* **2011**, *23* (5), 705−710.
(65) Rudolph, W. W.; Mason, R.; Pye, C. C. Aluminium(III) hydration in aqueous solution. A Raman spectroscopic investigation and an ab initio molecular orbital study of aluminium(III) water clusters. *Phys. Chem. Chem. Phys.* **2000**, *2* (22), 5030−5040.

https://doi.org/10.1021/acs.langmuir.4c02751
Langmuir 2024, 40, 20284−20293

(66) Lanzani, G.; Seitsonen, A. P.; Iannuzzi, M.; Laasonen, K.; Pehkonen, S. O. Isomerism of Trimeric Aluminum Complexes in Aqueous Environments: Exploration via DFT-Based Metadynamics Simulation. *J. Phys. Chem. B* **2016**, *120* (45), 11800−11809.
(67) Guo, L.; Xia, Y.; Jiao, X.; Chen, D. Ab Initio Molecular Dynamics Study of the Proton Transfer in Hydroxyl Ion-Induced Hydrolysis of Aluminum Monomers. *J. Phys. Chem. B* **2023**, *127* (33), 7342−7351.

https://doi.org/10.1021/acs.langmuir.4c02751
Langmuir 2024, 40, 20284−20293